Journal of Power Sources 194 (2009) 1089–1093

Contents lists available at ScienceDirect

Journal of Power Sources

journal homepage: www.elsevier.com/locate/jpowsour

Short communication

Low temperature synthesis of flower-like $ZnMn_2O_4$ superstructures with enhanced electrochemical lithium storage

Lifen Xiao, Yanyan Yang, Jia Yin, Qiao Li, Lizhi Zhang*

Key Laboratory of Pesticide & Chemical Biology of Ministry of Education, College of Chemistry, Central China Normal University, Wuhan 430079, People's Republic of China

ARTICLE INFO

Article history:
Received 21 April 2009
Received in revised form 12 June 2009
Accepted 15 June 2009
Available online 24 June 2009

Keywords:
Zinc manganate
Anode
Lithium-ion batteries
Solvothermal
Flower-like superstructure

ABSTRACT

In this communication, flower-like tetragonal $ZnMn_2O_4$ superstructures are synthesized by a facile low temperature solvothermal process. Characterizations show that these $ZnMn_2O_4$ superstructures are well crystallized and of high purity. The product exhibits an initial electrochemical capacity of 763 mAh g^{-1} and retains stable capacity of 626 mAh g^{-1} after 50 cycles. Its stable capacity is significantly higher than that of nanocrystalline $ZnMn_2O_4$ synthesized by a polymer-pyrolysis method. It is found that the higher capacity retention can be attributed to three-dimensional superstructural nature of the as-prepared flower-like $ZnMn_2O_4$ material. This study suggests that the solvothermally synthesized flower-like $ZnMn_2O_4$ is a promising anode material for lithium-ion batteries.

1. Introduction

Lithium-ion batteries have rapidly conquered the consumer market of advanced portable electronics in recent years and are now considered as the next generation power sources for future electric vehicles (EVs), hybrid EVs and plug-in hybrid EVs [1–5]. Graphite as lithium intercalation anode is currently most used, but its gravimetric capacity is inevitably limited to 372 mAh g^{-1}. Lithium metal alloys, especially those composed of group IV A elements (Si, Sn, etc.) have been extensively investigated as potential high capacity anode materials because they are able to accommodate large amounts of lithium ($Li_{4.4}Si$: 4200 mAh g^{-1}, $Li_{4.4}Sn$: 994 mAh g^{-1}). But all the alloy processes have suffered sever volumetric changes, which result in cracking and pulverization of the materials and poor cyclability [6–9].

Recently, nanostructured 3d-transition metal oxides have received attention as possible anodic alternatives for lithium-ion batteries [10–17]. These transition metal oxides (especially Mn, Fe, Co, Ni, Cu, etc.) have no free interstitial sites within their crystallographic structure to host lithium and do not form alloys with lithium. However, they can react reversibly with lithium according to a process termed conversion reaction: $M_xO_y + 2ye^- + 2yLi^+ = xM^0 + yLi_2O$. This electrode reaction leads to form composite materials consisting of metallic nanograins (M^0) dispersed into amorphous Li_2O matrix. Owing to the nanometric nature of this composite, such reactions are highly reversible. The theoretical capacity offered by these reactions depends on the oxidation state of the 3d metals existed in the voltage range of interest. Thus, they are potential to provide high and constant lithium storage capacities upon cycling (CoO: 700 mAh g^{-1}, Co_3O_4: 700 mAh g^{-1}, $ZnCo_2O_4$: 900 mAh g^{-1}).

In view of the toxicity and high cost of Co, inexpensive and environment friendly electrode materials such as Fe- and Mn-based oxides may be more popular and promising. Recently, we utilized a polymer-pyrolysis method to synthesize nanocrystalline $ZnMn_2O_4$ as a novel lithium-storage material. As cycled at 100 mA g^{-1} between 0.01 and 3.0 V, the nanocrystalline $ZnMn_2O_4$ electrode delivered a high initial reversible capacity of 776 mAh g^{-1} and retained a stable capacity of 569 mAh g^{-1} after 50 cycles [18]. In this communication, we develop a solvothermal synthetic method to prepare flower-like $ZnMn_2O_4$ superstructures at a temperature of 160 °C. The reaction temperature is much lower than that (600 °C) of the polymer-pyrolysis synthetic method, suggesting the solvothermal method in this study is more promising for industrial production of this novel lithium-storage material. More interestingly, the flower-like $ZnMn_2O_4$ superstructures could remain a stable capacity of 626 mAh g^{-1} after 50 cycles, significantly higher than that of nanocrystalline $ZnMn_2O_4$ synthesized with a polymer-pyrolysis method.

* Corresponding author. Tel.: +86 27 67867535; fax: +86 27 67867535.
E-mail address: zhanglz@mail.ccnu.edu.cn (L. Zhang).

0378-7753/$ – see front matter © 2009 Elsevier B.V. All rights reserved.
doi:10.1016/j.jpowsour.2009.06.043

2. Experimental

2.1. Synthesis

$ZnMn_2O_4$ were prepared by a low temperature solvothermal method. All of the reactants and solvents were analytical grade and were used without any further purification. In a typical procedure, 0.5 mmol of $Zn(NO_3)_2{\cdot}6H_2O$, 1.0 mmol of $Mn(NO_3)_2$, 0.5 mmol of citric acid and 0.25 mmol cetyltrimethylammonium bromide (CTAB) were added into 15 mL of anhydrous ethanol. The reaction mixture was vigorously stirred for 3 h and then transferred into a Teflon-lined stainless-steel autoclave with a capacity of 22 mL for solvothermal treatment at 160 °C for 48 h. After the autoclave had cooled down to room temperature naturally, the product was centrifuged, washed with anhydrous ethanol several times to remove alkaline salt and surfactants remained in the final products, and finally dried under vacuum at 100 °C for 12 h for use.

2.2. Characterization

X-ray diffraction (XRD) patterns of the samples were recorded on a Shimadzu XRD-6000 diffractometer (Cu Kα radiation). Data were recorded at a scanning rate of 4° min^{-1} ranging from 10° to 80°. Field emission scanning electron microscopy (SEM) was performed on a JSM-5600 scanning electron microscope. Transmission electron microscopy (TEM) and high-resolution transmission electron microscopy (HRTEM) were done using JEM-2010FEF instruments at an accelerating voltage of 200 kV.

2.3. Electrochemical measurement

The composite electrodes consisted of 80% $ZnMn_2O_4$, 12% acetylene black and 8% poly(tetrafluoroethylene) by weight and prepared by roll-pressing the mixture into an electrode film, then pressing the electrode film onto an nickel net. The testing cells had a typical three-electrode construction using lithium foil as both counter electrode and reference electrode, polypropylene microporous membrane as separator and 1 M $LiPF_6$ dissolved in ethylene carbonate (EC), dimethyl carbonate (DMC) and ethylene methyl carbonate (EMC) (1:1:1, v/v/v) as the electrolyte. The cells were assembled in an argon-filled glove box. The charge–discharge measurements were carried out using a BTS-55 Battery charger at 100 mA g^{-1} in a range of 3.0–0.01 V vs. Li/Li^+. The cyclic voltametric measurements were performed on a CHI660A Electrochemical Workstation at a scan rate of 0.1 mV s^{-1} in a range of 3.0–0.01 V vs. Li/Li^+.

3. Results and discussion

XRD was first used to analyze the as-prepared sample synthesized with the solvothermal method at a temperature as low as 160 °C (Fig. 1). The sharp reflections can be unambiguously indexed as tetragonal $ZnMn_2O_4$ with space group of $I4_1/amd$. The lattice parameters evaluated as $a = 5.7225$ Å, $c = 9.2513$ Å, are well accorded with the reported data (JCPDS File No. 24-1133). No characteristic peaks are observed for other impurities indicating the high purity of the sample. Therefore, the solvothermal method developed in this study is very promising for the synthesis of $ZnMn_2O_4$ in view of energy saving.

The morphologies of the as-prepared $ZnMn_2O_4$ sample obtained in this work were examined by using FE-SEM, TEM, SAED and HRTEM analysis. As shown in the FE-SEM image in Fig. 2a, the as-obtained $ZnMn_2O_4$ looks like clusters of flower-like spheres with submicron sizes. After magnification, it is found that these flower-like spheres are composed of numerous randomly oriented tapering nanorods with diameters around 50–100 nm as the "flower petals"

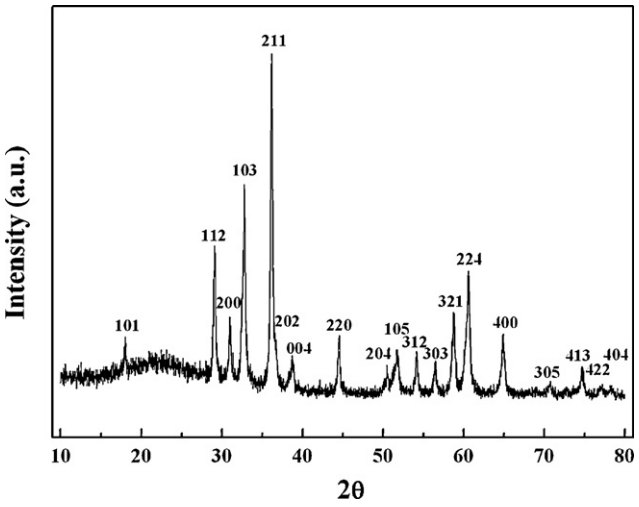

Fig. 1. XRD pattern of the as-prepared flower-like $ZnMn_2O_4$.

(Fig. 2b). The broken spheres show the interior of the spheres piled with crystalline $ZnMn_2O_4$ nanoparticle aggregates (Fig. 2c). The height of the petals is estimated as around 300 nm. The TEM image in Fig. 2d further confirms the superstructure of flower-like spheres and the diameters of the "flower petals" are several tens of nanometers, agreeing with the SEM observations. The SAED pattern on a single nanorod petal comprises diffused concentric rings (inset in Fig. 2d), indicative of polycrystalline structure of the petals. The diameters of the diffraction rings are in good agreement with the simulated Miller indices of $ZnMn_2O_4$. The HRTEM image (Fig. 2e) of the petal tip reveals that the nanoparticles in the $ZnMn_2O_4$ nanorods are highly crystallized, consistent with SAED result. The interplanar spacing are calculated to be 4.85, 2.99 and 2.47 Å, matching well with the (1 0 1), (1 1 2) and (2 0 0) planes respectively in the XRD pattern. Therefore, we conclude that the solvothermal synthetic method is able to prepare well-crystallized $ZnMn_2O_4$ nanophase at a temperature as low as 160 °C.

We evaluated the electrochemical activity of flower-like $ZnMn_2O_4$ superstructure by means of cyclic voltammetric and galvanostatic cycling as shown in Fig. 3. It shows that the CV curves and the discharge–charge profiles are qualitatively similar to those of nanocrystalline $ZnMn_2O_4$ synthesized with a polymer-pyrolysis method [18]. Fig. 3a gives the CV profiles at a scan rate of 0.1 mV s^{-1} in the voltage range of 0.01–3 V vs. Li/Li^+. As can be seen, the first CV curve has very different reduction profile in the cathodic sweep and identical oxidation peak positions in the anodic sweep compared with the successive scans. The quite different shape during the first lithium intercalation reveals that the initial reduction process displays a very different reaction mechanism from subsequent ones. The first cathodic scan shows a shoulder peak at ~0.6 V which may be ascribed to the irreversible decomposition of the solvent in the electrolyte to form the solid electrolyte interphase (SEI). This is followed by an intensive peak at ~0.2 V which may be attributed to the irreversible reduction of $ZnMn_2O_4$ with the concomitant crystal structure destruction to form metallic nanograins (M^0) dispersed into amorphous Li_2O matrix. The first anodic sweep shows two oxidation peaks at around 1.2 and 1.5 V can be associated with the oxidation of Mn and Zn nanograins to MnO (~1.2 V) [13] and ZnO (~1.5 V)[12], respectively. From the second scan onward, only a reduction peak located at around 0.4 V is observed.

Fig. 3b presents the discharge–charge curves of the flower-like $ZnMn_2O_4$ electrode cycled between 0.01 and 3.0 V at a constant current density of 100 mA g^{-1}. The voltage plateau is reflected as peaks in the CV curves. The discharge curve obtained over the first cycle is different from those of the following ones. The first

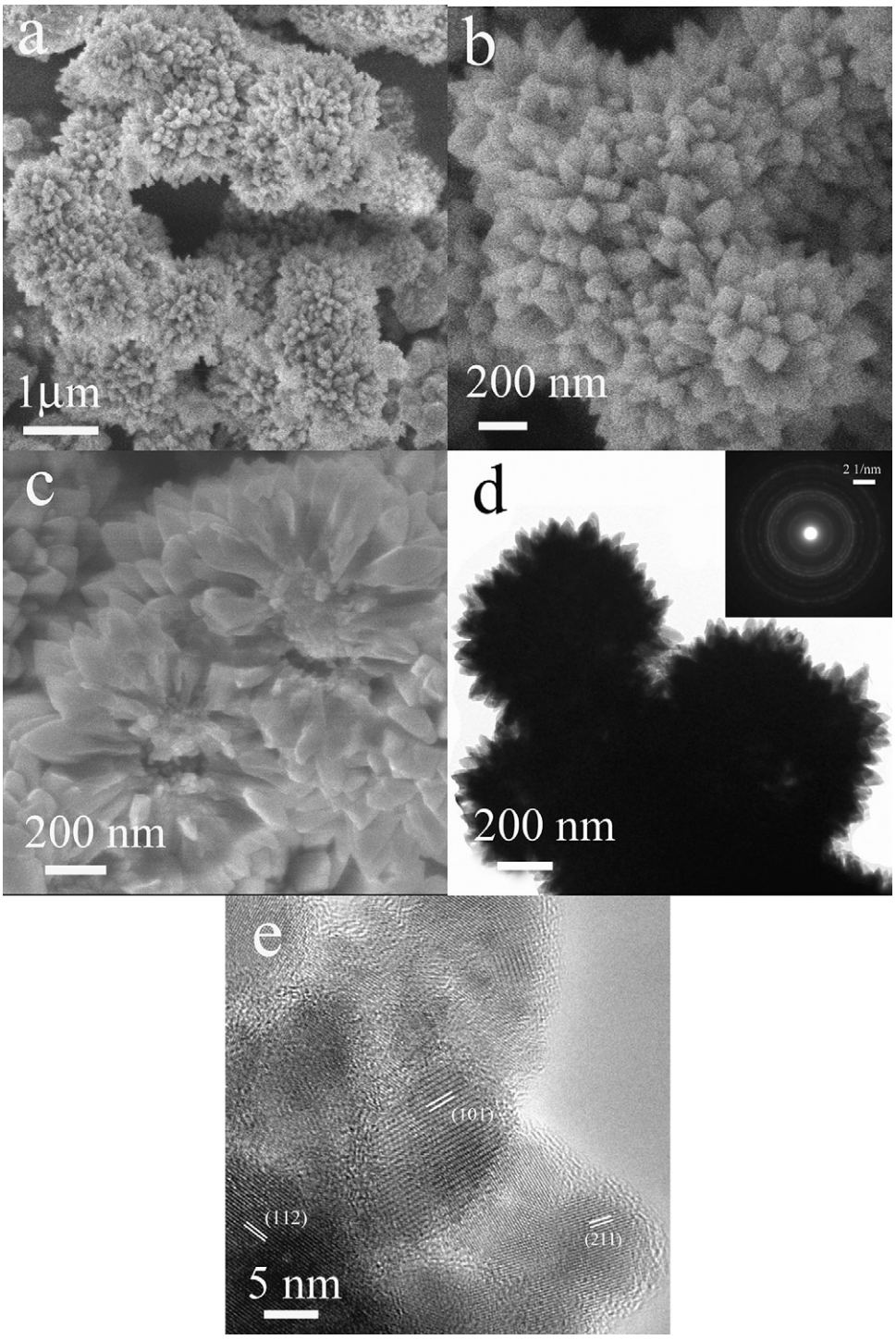

Fig. 2. (a–c) SEM, (d) TEM image and (e) HRTEM images of the as-prepared flower-like $ZnMn_2O_4$. The inset of (d) is the SAED pattern of the as-prepared $ZnMn_2O_4$.

discharge profile comprises a small plateau at about 0.6 V, then a wide plateau at about 0.4 V and a continuous slope to the lower cut off voltage to consume an overall capacity of 1350 mAh g^{-1}. The electrochemical process occurring during the first discharge is expected to be the reduction of $ZnMn_2O_4$ into Mn^0 and Zn^0 according to Eq. (1). Besides, Zn^0 also can reversibly react with Li to form Li–Zn alloy (1:1) according to Eq. (2) to contribute to the discharge capacity, though the LiZn alloying–dealloying process cannot be clearly detected as peaks on CVs or plateaus on charge–discharge curves possibly because it occurs through many stages like $LiZn \leftrightarrow LiZn_2 \leftrightarrow Li_2Zn_5$ [19]. In order to confirm this structural change, the ex situ XRD analysis was conducted on the electrodes after discharged and charged to selected voltage as described in Fig. 4. It shows that after the first discharge to 0.45 V, the crystalline peaks of $ZnMn_2O_4$ has already disappeared completely apart from the peaks arising from the Ni substrate and PTFE film. No peaks corresponding to metallic Mn and Zn or LiZn alloy were observed in the XRD pattern of the electrode after discharged to 0.01 V, which can be attributed to the nanoparticle nature of the electrochemically formed species, which are presumably smaller than the X-ray coherence length. This amorphous nature of the electrode material, once created during first dis-

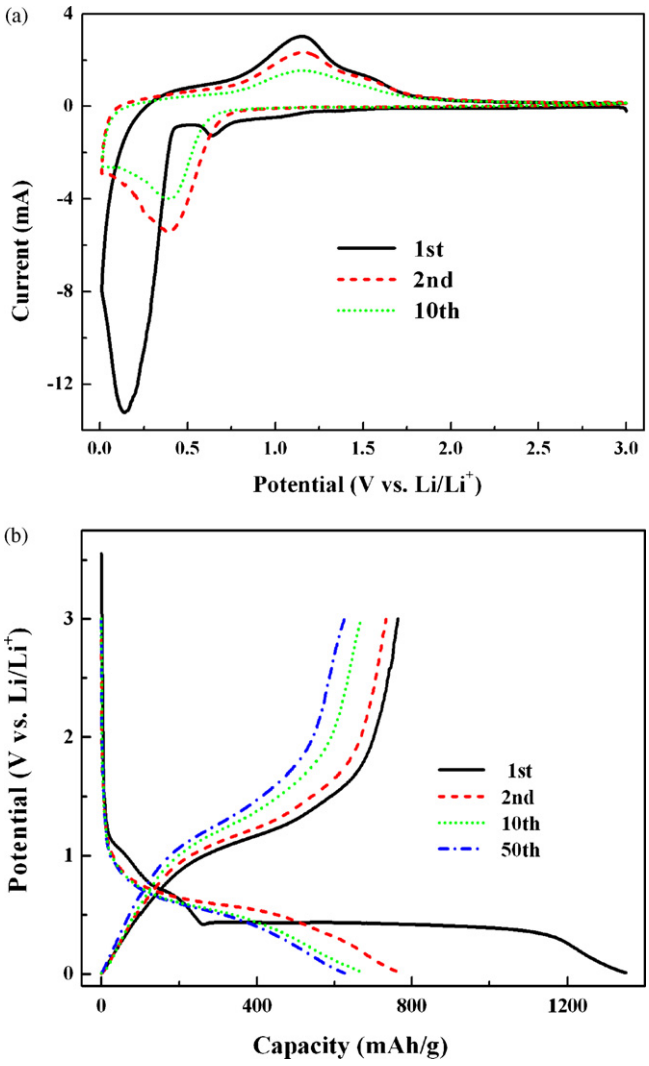

Fig. 3. (a) Cyclic voltammograms of the flower-like $ZnMn_2O_4$ electrode in the voltage range of 0.01–3.0 V at a scan rate 0.1 mV s^{-1} and (b) discharge–charge profiles of flower-like $ZnMn_2O_4$ electrode at 100 mA g^{-1} in the voltage range of 0.01–3.0 V.

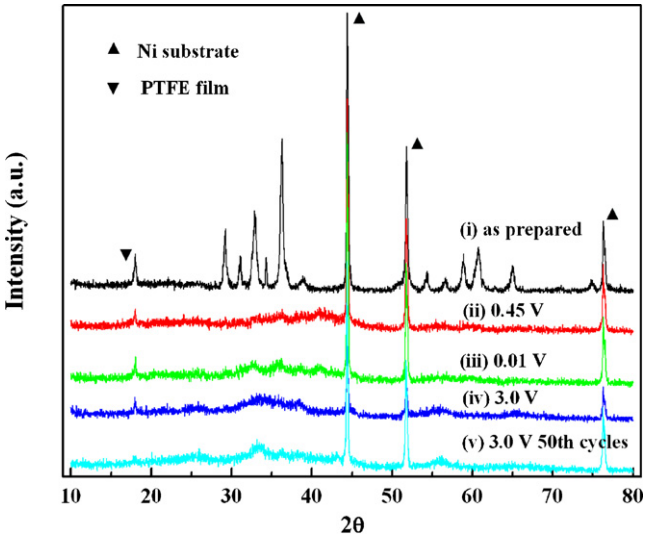

Fig. 4. Ex situ XRD patterns of the electrode, (i) as-prepared, (ii) discharged to 0.45 V, (iii) discharged to 0.01 V and (iv) charged to 3.0 V during the first cycle as well as (v) charged to 3.0 V after 50th cycles as labeled. The lines due to the nickel substrate and PTFE film are also shown.

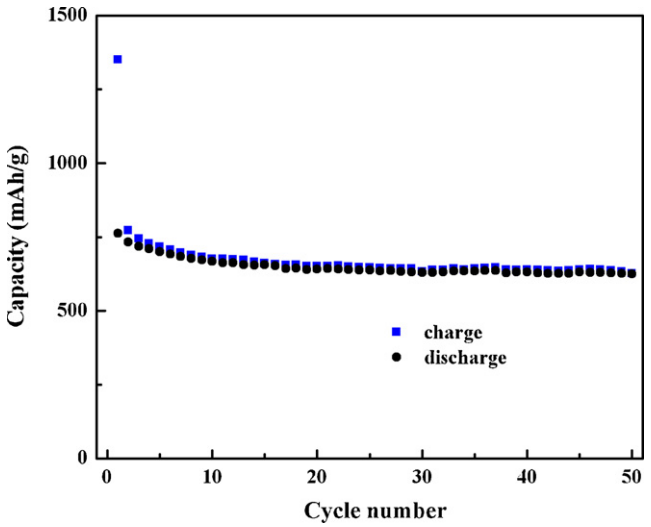

Fig. 5. Discharge–charge capacity vs. cycling number for the flower-like $ZnMn_2O_4$ electrode at 100 mA g^{-1} in the voltage range of 0.01–3.0 V.

charge, is preserved during following discharge and charge cycles as shown on electrode after 50 cycles. Beside, the above two equations would consume a capacity of 1008 mAh g^{-1}. The extra capacity of 342 mAh g^{-1} observed on the experiment should be ascribed to the solid–electrolyte interphase (SEI) formation due to the reaction of Li with the solvents. The first charge up to 3.0 V recovers a reversible capacity of 763 mAh g^{-1}, which match well with the theoretically achievable capacity of 784 mAh g^{-1} according to Eqs. (2)–(4). After the first cycle, reversible electrode reactions take place according to Eqs. (2)–(4), as the coulombic efficiency reach 95% in the second cycle and stabilizes at >98% after the sixth cycle.

$$ZnMn_2O_4 + 8Li^+ + 8e^- \rightarrow Zn + Mn + 4Li_2O \quad (1)$$

$$Zn + Li^+ + e^- \leftrightarrow LiZn \quad (2)$$

$$2Mn + 2Li_2O \leftrightarrow 2MnO + 4Li^+ + 4e^- \quad (3)$$

$$Zn + Li_2O \leftrightarrow ZnO + 2Li^+ + 2e^- \quad (4)$$

Fig. 5 shows the cycling performance of flower-like $ZnMn_2O_4$ superstructure electrode. It is found that the cycling behavior of the flower-like $ZnMn_2O_4$ superstructure electrode is very similar to the nanocrystalline $ZnMn_2O_4$ electrode prepared by polymer-pyrolysis method. Both electrodes show relatively fast reversible capacity loss during the initial 10 cycles, then exhibit stable cycling performance during the 10th to 50th cycles. However, during the first 10 cycles, the flower-like $ZnMn_2O_4$ electrode only lost 12% of its initial capacity, significantly less than that of 20% loss in nanocrystalline $ZnMn_2O_4$. In other words, the flower-like $ZnMn_2O_4$ superstructure electrode still remained a discharge capacity of 626 mAh g^{-1} after 50 cycles, much higher than that of 569 mAh g^{-1} of nanocrystalline $ZnMn_2O_4$. It is known that the fast capacity loss during the initial several cycles is attributed to the 'formation' or 'conditioning' of the electrode [20]. This phenomenon also has been observed in other oxide systems [21,22]. Therefore, we conclude that the three-dimensional superstructures of these flower-like spheres would be favorable to build stable SEI layer on the metal nanoparticles and establish intimate electric contact of the 'composite' with the current collector, and thus improve its electrochemical properties to a great extent.

4. Conclusions

In summary, we developed a low temperature solvothermal method to synthesize flower-like $ZnMn_2O_4$ superstructures. This

flower-like $ZnMn_2O_4$ superstructure electrode could exhibit an initial reversible capacity of 763 mAh g^{-1} cycled at 100 mA g^{-1} in the voltage range of 0.01–3.0 V and retained 626 mAh g^{-1} capacity after 50 cycles. Its stable capacity was significantly higher than that of nanocrystalline $ZnMn_2O_4$ synthesized with a polymer-pyrolysis method. The excellent electrochemical performance of flower-like $ZnMn_2O_4$ makes it a promising anode material for high-power lithium-ion batteries.

Acknowledgments

This work was supported by National Basic Research Program of China (973 Program) (Grant 2007CB613301), National Science Foundation of China (Grant 20777026), and Program for New Century Excellent Talents in University (Grant NCET-07-0352).

References

[1] J.M. Tarascon, M. Armand, Nature 414 (2001) 359.
[2] M. Armand, J.M. Tarascon, Nature 451 (2008) 652.
[3] P. Gibot, M. Casas-Cabanas, L. Laffont, S. Levasseur, P. Carlach, S. Hamelet, J.-M. Tarascon, C. Masquelier, Nat. Mater. 7 (2008) 741.
[4] P.G. Bruce, B. Scrosati, J.-M. Tarascon, Angew. Chem. Int. Ed. 47 (2008) 2930.
[5] B. Kang, G. Ceder, Nature 458 (2009) 190.
[6] M. Winter, J.O. Besenhard, M.E. Spahr, P. Novak, Adv. Mater. 10 (1998) 725.
[7] T. Li, Y.L. Cao, X.P. Ai, H.X. Yang, J. Power Sources 184 (2008) 473.
[8] Z. Chen, J. Qian, X. Ai, Y. Cao, H. Yang, J. Power Sources 189 (2009) 730.
[9] J. Hassoun, S. Panero, G. Mulas, B. Scrosati, J. Power Sources 171 (2007) 928.
[10] P. Poizot, S. Laruelle, S. Grugeon, L. Dupont, J.M. Tarascon, Nature 407 (2000) 496.
[11] P.G. Bruce, B. Scrosati, J.-M. Tarascon, Angew. Chem. Int. Ed. 47 (2008) 2.
[12] Y. Sharma, N. Sharma, G.V.S. Rao, B.V.R. Chowdari, Adv. Funct. Mater. 17 (2007) 2855.
[13] D. Pasero, N. Reeves, A.R. West, J. Power Sources 141 (2005) 156.
[14] Q. Fan, M.S. Whittingham, Electrochem. Solid-State Lett. 10 (2007) A48.
[15] L. Yu, H. Yang, X. Ai, Y. Cao, J. Phys. Chem. B 109 (2005) 1148.
[16] X.P. Gao, J.L. Bao, G.L. Pan, H.Y. Zhu, P.X. Huang, F. Wu, D.Y. Song, J. Phys. Chem. B 108 (2004) 5547.
[17] B.M.V. Reddy, T. Yu, C.H. Sow, Z.X. Shen, C.T. Lim, G.V. Subba Rao, B.V.R. Chowdari, Adv. Funct. Mater. 17 (2007) 272.
[18] Y. Yang, Y. Zhao, L. Xiao, L. Zhang, Electrochem. Commun. 10 (2008) 1117.
[19] J. Wang, P. King, R.A. Huggins, Solid State Ionics 20 (1986) 185.
[20] G. Binotto, D. Larcher, A.S. Prakash, R.H. Urbina, M.S. Hegde, J.M. Tarascon, Chem. Mater. 19 (2007) 3032.
[21] Y. Sharma, N. Sharma, G.V.S. Rao, B.V.R. Chowdari, Electrochim. Acta 53 (2008) 2380.
[22] Y. Sharma, N. Sharma, G.V.S. Rao, B.V.R. Chowdari, J. Power Sources 173 (2007) 495.